Hydrogen-induced surface structuring of a cubic boron nitride (100) face studied by low-energy electron diffraction and electron spectroscopic techniques

Kian Ping Loh, Isao Sakaguchi, and Mikka Nishitani-Gamo
Core Research for Evolutional Science and Technology (CREST) of Japan Science and Technology Corporation (JST), c/o National Institute for Research in Inorganic Materials (NIRIM), 1-1 Namiki, Tsukuba, Ibaraki 305-0044, Japan

Takashi Taniguchi
National Institute for Research in Inorganic Materials (NIRIM), 1-1 Namiki, Tsukuba, Ibaraki 305-0044, Japan

Toshihiro Ando*
Core Research for Evolutional Science and Technology (CREST) of Japan Science and Technology Corporation (JST), c/o National Institute for Research in Inorganic Materials (NIRIM), 1-1 Namiki, Tsukuba, Ibaraki 305-0044, Japan
(Received 11 September 1997)

The surface structure and secondary-electron-emission fine structure of single-crystal cubic boron nitride (100), exposed to hydrogen-plasma or argon-ion sputtering, was studied *in situ* with low-energy electron diffraction, secondary-electron-emission spectroscopy, electron-energy-loss spectroscopy, and Auger electron spectroscopy. Low-energy argon irradiation is capable of disrupting local ordering on the cubic boron nitride surface and to transform the near-surface region into sp^2-type bonding. The effect of hydrogen-plasma treatment is to etch the sp^2 amorphous layer away and regenerate sp^3 crystallinity on the surface. However, prolonged hydrogen-etching results in the faceting of the (100) face and changes surface symmetry from (100) 2×1 into (111) 1×1. The secondary-electron-emission spectra of cubic boron nitride were measured in the 0–50-eV electron kinetic-energy range in order to identify fine structures related to conduction-band states. These fine structures are found to be highly sensitive to long-range order, and their occurrence is characteristic of crystal perfection. The effect of cumulative argon sputtering is to degrade the secondary-electron-emission fine structures and suppress the secondary-electron yield. The excitation of the cubic boron nitride bulk plasmon at 36.8-eV electron loss energy is identified as the primary true secondary-electron production channel. Suppression of the bulk plasmon due to near-surface disorder results in the degradation of secondary-electron production from the surface. In contrast, hydrogen-plasma treatment of the amorphorized surface regenerates the bulk plasmon, the secondary-electron-emission fine structures as well as the total secondary-electron yield. The results provide strong evidence that the secondary-electron emission from surfaces is a sensitive function of near-surface order. [S0163-1829(98)05812-3]

I. INTRODUCTION

Despite the immense interest in cubic boron nitride (c-BN) because of its technological promise[1] as a superhard, chemically inert, wide-band-gap material, there are practically no experimental insights into the surface structure or reactivities of the c-BN surface. The biggest problem facing c-BN research is the lack of high-quality semiconducting single-crystal material, whereby surface and bulk properties can be evaluated adequately. Most of the surface studies involving c-BN to date were based on polycrystalline,[2] nanocrystalline,[3] or sometimes nonstoichiometric B_xN_y materials. Understanding the surface structure and reactivities of c-BN is essential toward developing the epitaxial growth of c-BN on other materials,[4,5] as well as the use of c-BN as a substrate for diamond heteroepitaxy.[6] For example, knowledge of the surface chemistry of atomic hydrogen and halogens on diamond has motivated research into potentially more efficient growth methods based on halogen-assisted chemical vapor deposition[7] as well as chemical beams.[8] In addition, the band gap of c-BN ($\sim$6.3 eV) is wider than that of diamond, and it can potentially show superior negative electron affinity-related electron-emission properties, as demonstrated recently by the comparative field-emission studies of polycrystalline c-BN and diamond.[9] Electron emission is critically dependent on surface crystallographic orientation as well as the nature of chemical species terminating the crystal face.[10] From a fundamental viewpoint, research on c-BN is highly interesting because the material is intermediate between diamond, SiC, and III-V compounds. Unlike diamond, the bonds in c-BN are hetero-polar and the differences in ionic radii is 20%. Calculations show that the preferred form of surface structure is a SiC-type of 2×2 bridging reconstruction.[11] X-ray-diffraction intensity analysis shows that there is a charge transfer of about $0.4e$ from the B to N atoms,[12] which means its polarity is rather similar to III-V compound materials, and would provide properties different from that of diamond with symmetric electron distribution along the C-C bonds. At the c-BN surface, atomic valencies can allow three-fold coordination of either a boron or nitrogen dimer atom without any dangling bonds. This is in contrast to the diamond surface where the (111) 1×1 or (100) 2×1 surface structure has to be maintained by monohydride termination to prevent the collapsing of the surface into π bonds.[13,14] Finally, depending on whether the surface is terminated by nitrogen or boron, the chemical reactivities

and electronic properties may differ. For example, during the heteroepitaxial growth of diamond on *c*-BN, nucleation is observed to proceed selectively on the boron-terminated surface.[6] The different reactivities of the boron- and nitrogen-terminated surface manifest in wet-etching behaviour as well. Due to the polarity difference between the B and N face ($B^{\partial+}N^{\partial-}$), the B face reacts rapidly with OH^--based etchants, while the N face reacts rapidly with H^+-based etchants, leaving behind predominantly inert N or B etch-pit faces, respectively.[15] In this study, in order to investigate the etching capability of atomic hydrogen on BN sp^2 phases, the *c*-BN (100) sample was amorphorized sequentially in a controlled manner and then treated with hydrogen plasma. Our motivation is based on the consideration that atomic hydrogen can assume the role of an sp^2 etchant as well as a sp^3 phase promoter during the chemical vapor deposition (CVD) of diamond; therefore it is interesting to consider the interactions of atomic hydrogen with *c*-BN. Hydrogen termination of the diamond surface has also been known to produce a negative electron affinity condition,[16] which enhances the escape probability of secondary electrons from the surface. In that context, we record the secondary-electron-emission spectra during hydrogen-plasma treatment and cumulative argon sputtering of the surface in order to understand the dependence of the secondary-electron-emission characteristics on the *c*-BN surface condition.

II. EXPERIMENT

The Be-doped *c*-BN (100) crystal ($2\times2\ mm^2$) used in this study was grown heteroepitaxially on diamond (100) under high-temperature and high-pressure conditions using the temperature gradient method as reported previously.[17] Surface science studies were carried out in an Auger microprobe system equipped with dedicated electron optics for performing scanning electron microscopy (SEM), ion-beam profiling, secondary-electron-emission spectroscopy (SEE), electron-energy-loss spectroscopy (EELS), and Auger electron spectroscopy (AES). SEE measurements were performed using a field-emission-type electron gun capable of high spatial resolution (10-nm spot size) and a 100-mm radius concentric hemispherical analyzer utilizing pulse-counting, multichannel detection. Argon sputtering was performed *in situ* with a rastered ion beam at 0.5–2 KeV, and at a beam current of 40–70 nA. All focusing for electron spectroscopy and ion beam etching was fine tuned with the help of real-time secondary electron imaging of the sample. Secondary electrons were excited by primary beam energy of 1 KeV and with a beam current of 10 nA on a spot size of 100 μm, and were detected by the analyzer at normal emission using a constant retardation ratio (CRR) mode of 0.15 EELS was performed using 1-KeV primary beam and with the analyser at a fixed pass energy of 20 eV. The full width at half maximum of the primary peak was less than 2 eV. Low-energy electron diffraction (LEED) was performed in a second UHV chamber equipped with four-grid retarding-field electron optics. The second UHV chamber is connected to a microwave CVD system where the sample can be introduced in vacuum for treatment with pure hydrogen plasma, utilizing a microwave power of 800 W, a hydrogen pressure of 5.3 kPa, a flow rate of 400 ml min^{-1}, and a substrate temperature between 650 and 750 °C. The term ''as-received'' in the context of our sample means as-grown *c*-BN crystal that had been subjected to polishing with diamond grit to obtain an optical finish and ultrasonication in ethanol bath before its introduction into the UHV chamber. Surface compositional analysis by AES of the as-received *c*-BN (100) sample revealed about 10% carbon contamination on the surface, and with B:N elemental ratios observing 1:1 stoichiometry. The electronic spectra of a commercially available highly oriented pyrolytic hexagonal BN (*h*-BN) sample were also recorded for comparison.

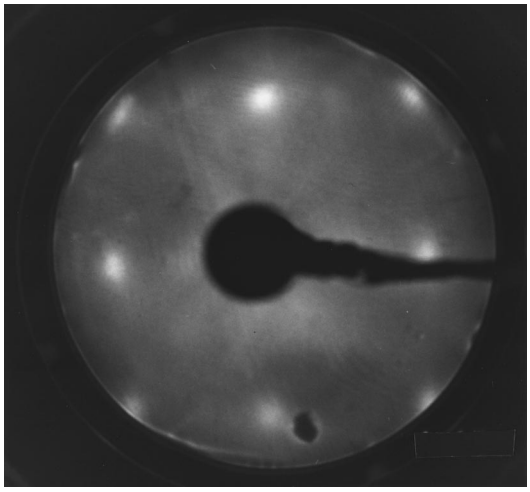

FIG. 1. LEED pattern of an as-received *c*-BN (100) crystal showing (100) 1×1 at E_p (primary energy)=124 eV.

III. RESULTS

A. LEED

The LEED pattern of the as-received *c*-BN (100) is shown in Fig. 1 to reveal a 1×1 symmetry. Large, diffuse diffraction spots and a high background intensity are indicative of a poorly formed surface after polishing. There are two possibilities for the lack of a reconstructed superlattice of long-range order: the experimentally observed (100) 1×1 structure could either reflect the periodicity of the bulk material under a disordered surface, or it could reflect ideal bulk-terminated (100) surface. The *c*-BN (100) 1×1 surface was then treated with pure hydrogen-plasma for 45 mins at 750 °C. As a result, the four-fold symmetry square mesh in the LEED pattern of Fig. 1 is dramatically transformed into a very sharp, six-fold symmetry hexagonal mesh, as shown in Fig. 2(a). The 1×1 hexagonal reciprocal net is indicated in Fig. 2(b). The observed diffraction spots were concluded to originate from facets generated by hydrogen etching because of (i) the trajectory crossing of LEED spots as incident energy of the electron beam was varied, and (ii) the off-normal position of the reflected primary beam and generation of secondary electron patterns. The observed symmetry, hereby denoted as (111) 1×1, was found to be quite stable to further restructuring as the (111) 1×1 structure did not change upon further exposure to hydrogen plasma.

In order to obtain information on surface cleaning and regeneration, the same *c*-BN (100) sample exhibiting faceted

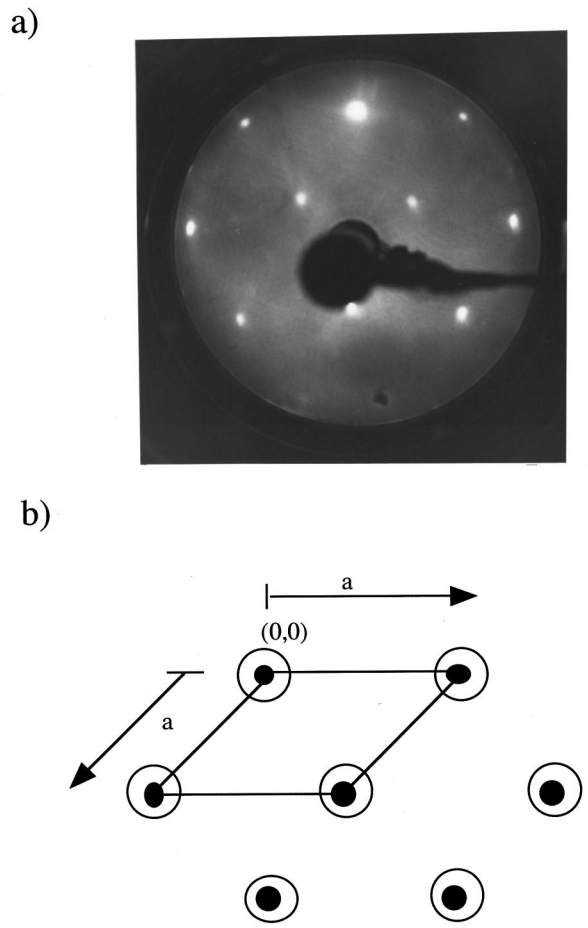

FIG. 2. (a) LEED pattern showing sharp (111) 1×1 structure after the first hydrogen, plasma treatment for 45 min at 750 °C and $E_p = 150$ eV. (b) The 1×1 hexagonal net in reciprocal space. ○, first-layer surface atoms; ●, second-layer (bulk) atoms.

(111) 1×1 surface symmetry was subjected to low energy (500 eV) argon sputtering. The diffraction pattern vanished following such a treatment for 10 min, suggesting a loss of the long-range order. The argon-sputtered surface was then subjected to hydrogen-plasma treatment at 690 °C for 15 min. The intensities of the diffraction spots were regenerated following such a treatment, but the symmetry, as shown in Fig. 3(a), changed dramatically to that of (100) 2×1. The reciprocal net is illustrated in Fig. 3(b). Weak half-order spots could be seen in the ⟨010⟩ direction but absent from the orthogonal ⟨100⟩ direction. This is evident of the fact that in real space, the surface atoms have periodicity twice that of the bulk in one crystallographic orientation, which is consistent with a surface (100) 2×1 reconstruction. To investigate the effect of prolonged hydrogen-plasma treatment on the surface structure, the (100) 2×1 surface was further treated by hydrogen plasma at a higher temperature of 750 °C for 15 min. The LEED pattern as shown in Fig. 4 reveals the disappearance of the half-integral spots, so that the surface grating appears to be similar to that of the truncated bulk (100) 1×1. Finally, after exposing the surface to hydrogen-plasma treatment at 750 °C for another 20 min, the symmetry of the diffraction spots once again transformed to a (111) 1×1 pattern as shown in Fig. 5, which is evident of the restructuring of the cubic (100) face into (111) facets by hydrogen-plasma etching.

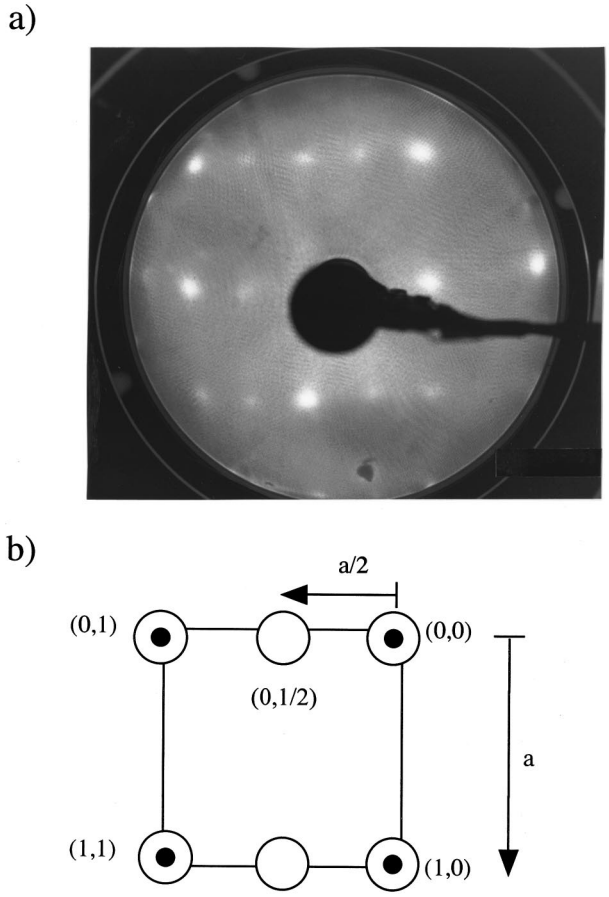

FIG. 3. (a) LEED pattern showing (100) 2×1 structure after hydrogen-plasma treatment of the amorphorized surface (argon sputtered) at 690 °C for 15 min; $E_p = 178$ eV. (b) The 2×1 net in reciprocal space ○, first-layer surface atoms, ● second-layer (bulk) atoms.

B. SEE results

Prior to recording the SEE spectrum, the *c*-BN (100) sample was treated with hydrogen-plasma at 690 °C to etch away surface carbon contamination so that, within the sensitivity of AES analysis, the chemical composition of the surface consisted of only boron and nitrogen observing stoichio-

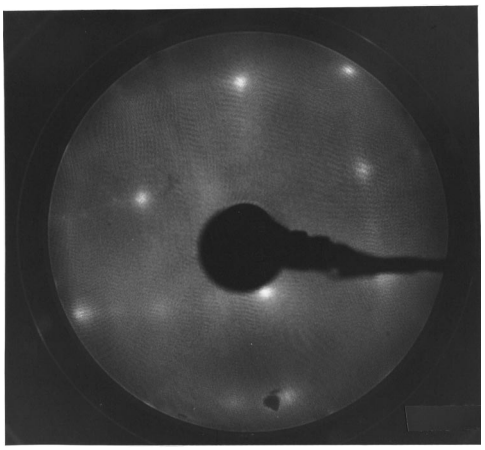

FIG. 4. LEED pattern showing (100) 1×1 structure following further hydrogen-plasma treatment of the (100) 2×1 surface (Fig. 3) at 755 °C for 15 min; $E_p = 189$ eV.

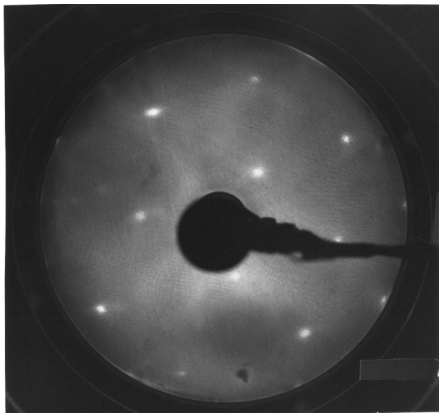

FIG. 5. LEED pattern showing the regeneration of the (111) 1×1 structure after a final hydrogen-plasma treatment of the (100) 1×1 surface (Fig. 4) at 750 °C for 20 min; $E_p = 160$ eV.

metric ratios. Figure 6 shows the SEE spectra collected for the c-BN sample from 0–50-eV absolute kinetic energy as a function of primary beam energy in the $N(E)$ vs E mode. The integrated intensity of these secondary electrons are commonly used in order to image surfaces in the SEM, and the total intensity of the secondary electron yield directly correlates with the brightness of the sample SEM image. As can be seen, between 1000- and 500-eV primary electron beam, the energy dependence of the secondary-electron yield consists of several well-defined peaks indicated as S_0, S_1, S_2, and S_3 in Fig. 6. To identify the true energy positions of the fine-structure peaks and to eliminate the background, the spectra in the integrated $N(E)$ mode were differentiated twice to obtain the $d^2(E)/d[N(E)]^2$ spectra, where the true energy positions can be read off from the negative maximum

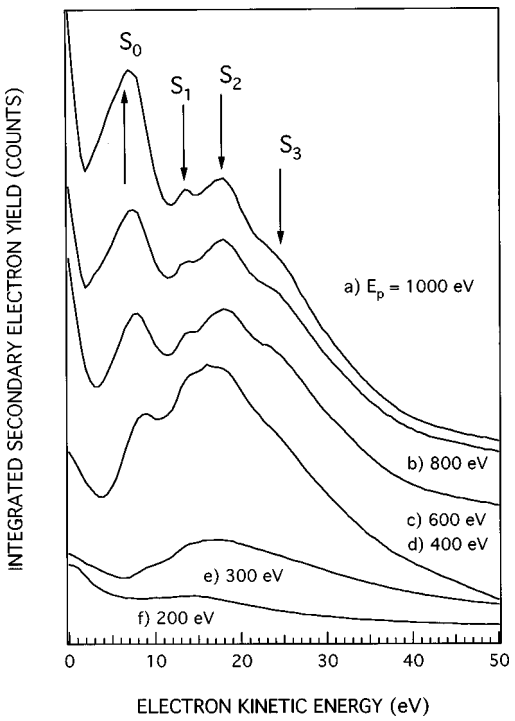

FIG. 6. SEE spectra of the c-BN (100) sample collected in the $N(E)$ vs E mode excited by different primary-electron energies as indicated.

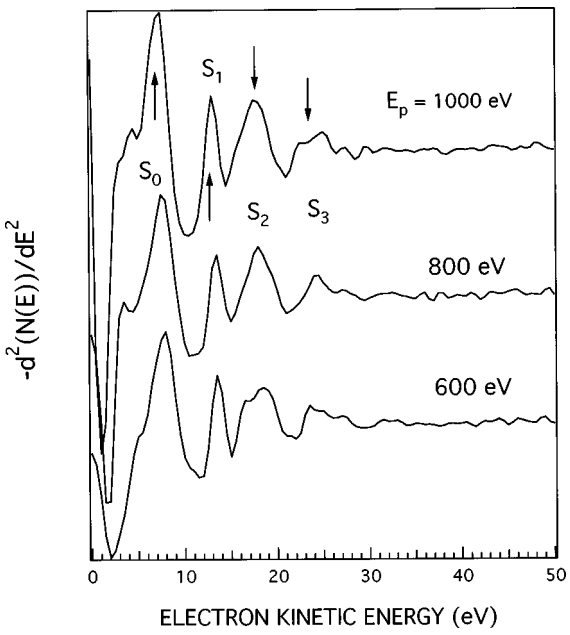

FIG. 7. SEE spectra of c-BN (100) as in Fig. 6, but collected in the negative of the double derivative mode.

$-d^2(E)/d[N(E)]^2$ as indicated in Fig. 7. The spectra in Fig. 7 were normalized for comparison. Varying the beam energy from 1000 to 600 eV did not affect the peak positions of S_0 (7.5 eV), S_1 (13 eV), S_2 (17 eV), and S_3 (24 eV). As the c-BN Fermi level is extrinsic and band bending may occur at the c-BN surface, it was not possible to measure the electron kinetic energy accurately with respect to the c-BN vacuum level from our study, and peak positions are simply quoted in absolute kinetic energies. These peaks were consistently well defined in terms of shapes and positions as the electron beam was scanned across the surface. Below a primary beam energy of 400 eV, the secondary-electron yield declined, and the resolution of the fine structures was lost in the $N(E)$ vs E mode.

The dependence of the SEE fine structures on crystal perfection was investigated by sequential low-energy argon ion sputtering of the c-BN sample in order to introduce defects gradually onto the surface. Ion sputtering has been known to amorphorize diamond[18] and c-BN.[2] The results of the cumulative argon sputtering are shown in Fig. 8 in the $N(E)$ vs E mode. Clearly, there is dramatic transformation in the SEE spectra for an argon sputtering time as short as 15 min, as the well-defined peaks S_1, S_2, and S_3 become smeared out in Fig. 8(b). The spectra as indicated by Fig. 8(c) and 8(d), and which correspond to longer 500-eV argon sputtering time suffer a gradual loss in secondary-electron yield. With higher-energy argon sputtering at 1–2 KeV, the total secondary-electron yield became drastically suppressed, along with the degradation of peak S_0 as shown in Figs. 8(f)–8(h). Further to cumulative argon sputtering, the surface was treated with pure hydrogen plasma for 20 min. As a result, the SEE fine structures and the total secondary-electron yield as shown in Fig. 8(i) dramatically recovered. The peak profiles in Fig. 8(i) are qualitatively similar to the initial unsputtered surface in Fig. 8(a), indicating strongly that hydrogenation of the surface is capable of regenerating

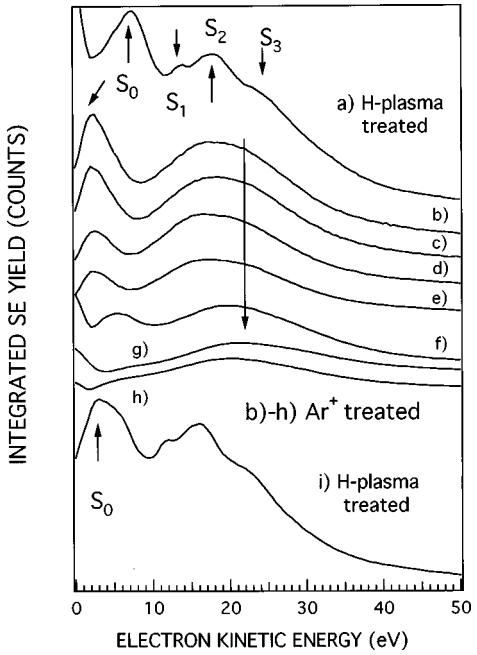

FIG. 8. Evolution of the SEE fine structures starting from a hydrogen-plasma treated c-BN (100) sample in (a); and after cumulative argon sputtering using an argon-ion beam of (b)–(d) 500 eV for 20, 40, and 60 min; (e) and (f) 1000 eV for 20 and 40 min; (g) 1500 eV, 20 min; and (h) 2000 eV, 20 min; (i) Showing the regeneration of the fine structures following a second hydrogen-plasma treatment for 20 min.

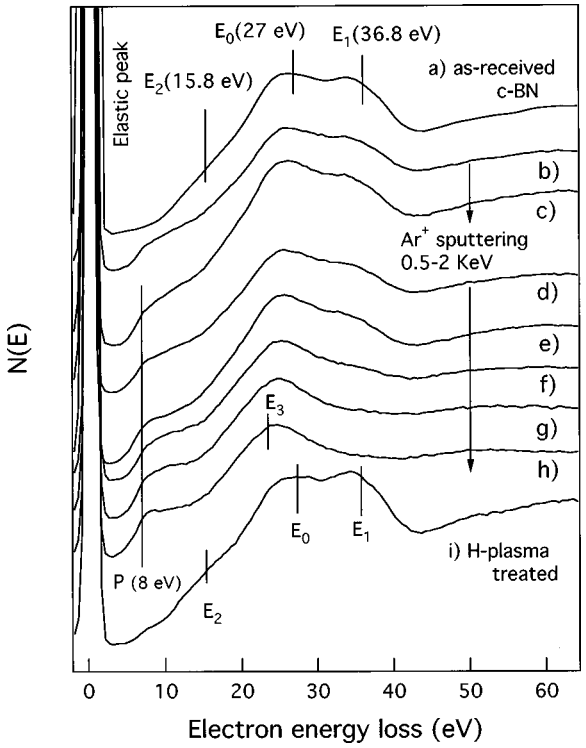

FIG. 9. Evolution in the EELS spectra starting from as-received sample in (a), and after cumulative argon sputtering using an argon-ion beam of (b)–(d) 500 eV for 20, 40, and 60 min; (e) and (f) 1000 eV for 20 and 40 min; (g) 1500 eV for 20 min; and (h) 2000 eV for 20 min. (i) After hydrogen-plasma treatment for 20 min.

initial-state crystallinity. It is also clear from the results that the SEE fine structures are meaningful expression of the surface crystalline integrity.

C. EELS

The SEE spectral evolution of c-BN during the entire sequence of surface modification was accompanied by EELS and high-resolution AES studies in order to understand the structural changes that effected the transformation in the SEE spectra. The peak positions were obtained after performing a linear background subtraction and Gaussian deconvolution to the energy-loss spectra. For the as-received sample, the EELS spectrum as shown in Fig. 9(a) collected in the $N(E)$ vs E mode, reveals two major plasmon peaks E_0 (27 eV) and E_1 (36.8 eV); the smaller peak E_2 at 15.8 eV is assignable to interband transition based on the reflectivity data of Phillip and Taft,[19] who reported a prominent peak at 14.5 eV. Following 500-eV argon sputtering for 15 min, a small shoulder labeled as P (8 eV) assignable to the $\pi \rightarrow \pi^*$ transition of sp^2 unsaturated bonds can be seen in Fig. 9(b), which grows in intensity with longer sputtering time. After further cumulative argon sputtering at higher argon beam energies, two further changes took place. First, the bulk plasmon peak E_1 (36.8 eV) is attenuated. Second, the peak E_0 (27 eV) moves to lower loss energy at position E_3 (23 eV). Comparing Fig. 9(h) with the EELS spectrum of pyrolytic hexagonal BN in Fig. 11(b) suggests that the effect of argon sputtering is to convert the sp^3 bonding on the surface into sp^2 bonding. This is evident in the suppression of plasmon peak E_1 and the shift of the plasmon peak E_0 to position E_3 (23 eV) closer to the bulk-plasmon peak (22.5 eV) of hexagonal BN, as well as the growth of π-bond peak P. The sp^3 phase can be regenerated however by hydrogen-plasma treatment as revealed in Fig. 9(i). The π-bond peak is completely suppressed following hydrogen-plasma treatment, along with the regeneration of the bulk plasmon peak E_1 (36.8 eV). Therefore we can identify plasmon peak E_1 as the fingerprint for good crystallinity in c-BN. It is worthwhile pointing out that while the lower-energy bulk plasmon peak E_0 (27 eV) is commonly observed for polycrystalline c-BN,[2] the higher energy E_1 (36.8 eV) peak is rarely reported despite being predicted by theoretical optical calculations.[20] This could be due to the fact that most of the surface studies to date involved polycrystalline or nanocrystalline BN material contaminated with carbon and oxygen.[2,21] In addition, argon bombardment has sometimes been used for surface ''cleaning'' of these polycrystalline material before recording the electron spectrum, which we have just demonstrated here to be effective in suppressing bulk plasmon peak E_1.

D. Auger *KVV*

High-resolution Auger *KVV* (core-valence-valence) spectra of boron are shown in Figs. 10(a) for the as-received surface, and Figs. 10(b)–10(e) for the argon-sputtered surface. No significant shift in the main Auger peak can be discerned along the whole course of argon sputtering, suggesting that charging effects were not present, due to the conductivity of our doped samples. The Auger peak positions are taken at the middle excursion of the maximum and minimum in the derivative curve to reveal the position of the

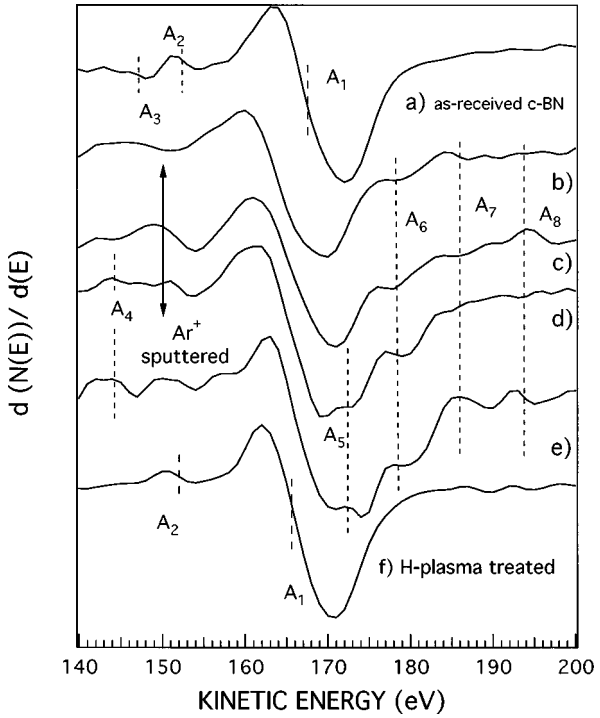

FIG. 10. High-resolution *KVV* Auger spectra for (a) as-received *c*-BN, and after cumulative argon sputtering using [(b) and (c)] 500 eV for 20 and 40 min; (d) 1000 eV for 20 min; and (e) 2000 eV for 20 min. (f) After hydrogen-plasma treatment for 20 min.

main Auger peak A_1 (167 eV) and one smaller peak at A_2 (152 eV). Both peaks were assigned in Ref. 2 to pyrolytic *c*-BN, considering the self-convolution of the valence-band density of states. After cumulative argon sputtering, the Auger spectra become richly structured with peaks at A_5 (172 eV), A_6 (177 eV), A_4 (144 eV), A_7 (184 eV), and A_8 (193 eV) as shown in Figs. 10(b)–10(e). These finer features are suppressed upon hydrogen-plasma treatment of the surface as shown in Fig. 10(f), along with a complete regeneration of the Auger peak profile before argon sputtering. The result is evident of the transformation of the local bonding environment of *c*-BN from sp^3 to sp^2 types characteristic of the hexagonal phase following 500–1500-eV argon sputtering. Following hydrogen-plasma treatment, these sp^2 phase was effectively etched. A comparison with the B-*KVV* Auger of hexagonal BN, shown in Fig. 11(c), reveals peaks A_4, A_5, and A_6 to be common to both the argon-sputtered *c*-BN and *h*-BN.

E. Pyrolytic hexagonal BN

The SEE, EELS, and AES spectra of pyrolytic hexagonal BN (*h*-BN) are provided for comparison in Figs. 11(a)–11(c). The SEE spectrum of *h*-BN is rather distinct from that of the *c*-BN; it consists of a sharp peak at 11 eV, which is due to the secondary-electron cascade before the vacuum level cutoff. In *c*-BN spectra, no discernible sharp low-energy cutoff near zero kinetic energy can be discerned for the SEE spectra (Fig. 6). Apparently, the vacuum level of *h*-BN is situated farther than that of *c*-BN from the spectroscopic Fermi constant. One reason is that the *h*-BN sample is more insulating than the Be-doped *c*-BN sample, and that

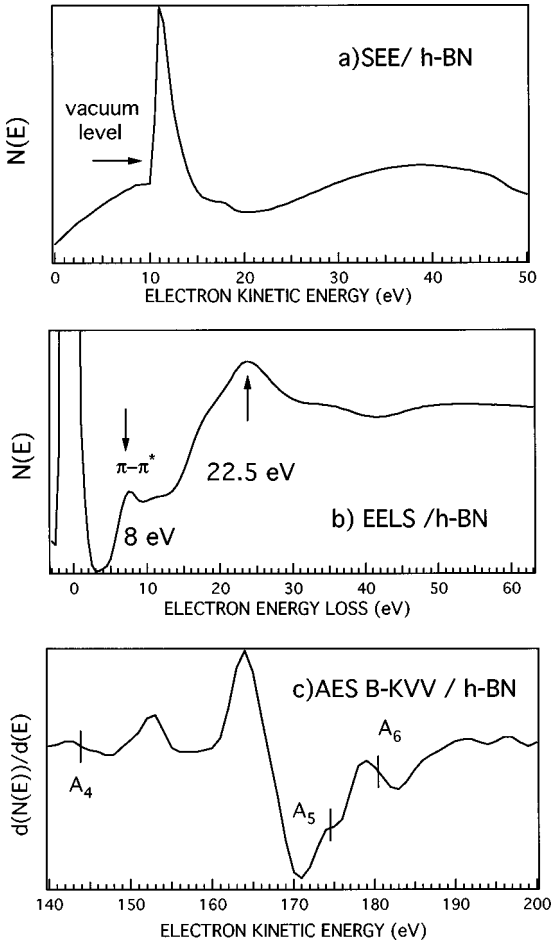

FIG. 11. Composite spectra showing (a) SEE, (b) EELS, and (c) Auger B-*KVV* of pyrolytic hexagonal BN.

charging occurred during electron spectroscopy, as verified by a shift in the low-energy cutoff with changes in the primary excitation energies. Another possibility is the occurence of a negative electron affinity condition for *c*-BN which can place the vacuum level below the conduction-band minimum. No distinct fine features can be seen in the SEE spectrum of *h*-BN collected in the $N(E)$ vs E mode compared to that of *c*-BN. The EELS spectrum of *h*-BN in Fig. 11(b) shows a distinct peak at 8 eV due to $\pi \rightarrow \pi^*$ transition of unsaturated bonds and a plasmon peak at 22.5-eV loss energy. The AES B-*KVV* spectrum of *h*-BN in Fig. 11(c) shows distinct peaks at A_4 (143 eV), A_5 (174 eV) and A_6 (181 eV) which are common to the argon-sputtered *c*-BN (Fig. 10).

IV. DISCUSSION

A. Surface structure

The ability of hydrogen plasma to smooth diamond surfaces is well-documented.[22,23] After treating the C(100) surface with pure hydrogen plasma, a sharp 2×1 LEED pattern can often be seen which is stable in air. Under more extreme conditions of etching time, plasma power, and substrate temperature, however, hydrogen plasma can result in increased faceting or roughening of the diamond surfaces.[24] At present, the mechanism responsible for smoothening or roughening

of the diamond surface by hydrogen is not understood. It is clear from the present study that hydrogen plasma can effectively etch and restructure the *c*-BN surface, with the extent of such restructuring, i.e., evolution of the LEED pattern, dependent on treatment time and substrate temperature. Interestingly, after moderate hydrogen-plasma treatment conditions (short treatment time, lower temperature of 690 °C), the *c*-BN (100) crystal was observed experimentally to adopt the (100) 2×1 surface symmetry (Fig. 3). Such a structure could be produced by parallel rows of boron or nitrogen dimers on the surface. The observation of a single-domain 2×1 structure also suggests that within the domain size (50 nm) defined by the electron-beam coherence width, the surface is terminated only by either nitrogen or boron, but not by both since the latter configuration will give rise to different domains orthogonal to each other and result in effectively a 2×2 or $2\times1/1\times2$ multidomain structure. With prolonged hydrogen-plasma etching, the surface becomes faceted, and a sequential transition of the surface symmetry from (100) 2×1 (Fig. 3) into intermediate (100) 1×1 (Fig. 4) and finally (111) 1×1 (Figs. 2 and 5) can be observed. The (111) 1×1 structure appears to be relatively stable to further restructuring at the plasma conditions employed in this work, although the reason for this is not clear at the moment. In view of the readiness at which the *c*-BN (100) surface can be structured, future attempts at cleaning or preparing a smooth *c*-BN (100) surface using microwave hydrogenplasma will require careful control of treatment time and substrate temperature.

B. Origins of *c*-BN SEE spectra

The SEE spectra have been demonstrated for many systems including graphite[25–27] and diamond,[18,28,29] and peaks in the fine structures have been shown to reflect high-energy conduction-band states in agreement with other spectroscopic techniques (i.e., inverse photoemission) sensitive to the empty density-of-states and band-structure calculations. The SEE fine structure may originate from (1) direct excitation of the valence-band electron by the primary electron, (2) by the population of unoccupied electronic states by cascade electrons (true secondaries), and (3) by means of the deexcitation channel for collective plasmon modes. Prior to their propagation into a vacuum, these secondary electrons occupy conduction-band states above the vacuum level in the crystal field; therefore, fine structure in the SEE spectrum will reflect the density of the unoccupied electronic states at the corresponding measured secondary-electron kinetic energies. As seen from Fig. 6, there is some dependence of the SEE spectrum on primary energy. The relative intensities of the peak S_0 (7.5 eV) to peak S_1 (13 eV) are observed to decrease from 1:0.6 to 1:1.8 as the primary beam is decreased from 1000 to 500 eV, along with a smearing out of the fine structures in the $N(E)$ mode. There is no change in the peak positions with changes in primary beam energy, indicating that the structures are derived from conduction-band states since a change in primary excitation energy will affect peak positions (kinetic energies) if the structures originate from the valence levels. The higher-energy primary beam has a higher efficiency in exciting electrons from deep-level states. These electrons undergo plasmon or Auger deexitation processes and can contribute to the structured secondary-electron peaks over the structureless secondary electron cascade observed using a lower-energy excitation beam. These SEE fine structures are sensitive fingerprints of the crystalline perfection on the *c*-BN surface. We find a correlation between the loss of the LEED diffraction spots and the smearing out of the SEE fine features following low-energy, short-time argon sputtering, together with the regeneration of the diffraction spots and spectral features following hydrogen-plasma treatment. It is instructive to compare the peaks in our SEE spectra in Fig. 7 with the theoretical valence band spectra of *c*-BN.[20,30,31] The energy values of the high-symmetry conduction-band states are referenced to the valence-band maximum (VBM) $\Gamma_{15,v'}$, which is set to zero energy value, as tabulated in Table I, along with possible assignments of the SEE peaks assuming integration of photoelectrons over the whole **k** space. The most likely assignment of peak S_0 (7.5 eV) is the conduction-band minimum (CBM) in *c*-BN. Similar observation of an intense peak at 5.5–6 eV with respect to the top of the valence band and attributable to the CBM has been reported for the SEE spectrum of diamond with an electron[28] or a photon[32] as the primary excitation source. In this case, if the CBM is above the vacuum level due to a negative electron affinity condition, electrons that are excited into the CBM can propagate into the vacuum with a band-gap energy of ~6–7 eV. The indirect band gap of *c*-BN has a the CBM at the $X_{1,C}$ symmetry point, located at 6.3 eV from the VBM. This means that 1.2 eV (7.5–6.3 eV) should be added to the as-measured absolute kinetic energies in our SEE spectra in order to reference them to the VBM. This allows us to assign the observed SEE peaks S_1-S_3 by comparison with the theoretically calculated band structure of *c*-BN,[30] as tabulated in Table I.

TABLE I. High-symmetry points from band-structure calculations of *c*-BN (Ref. 30).

Symmetry points	Energy values	SEE peaks assignment
$\Gamma_{15,v}$	0	···
$X_{1,c}$	6.3	S_0
$X_{3,c}$	11.3	···
$X_{5,c}$	21.9	S_3
$\Gamma_{1,c}$	12.6	S_1
$\Gamma_{15,c}$	11.4	···
$L_{1,c}$	18.5	S_2
$L_{3,c}$	13.4	···

C. Comparison with EELS and Auger spectroscopy

It is interesting to consider the correlation between the reduction in the integrated secondary-electron yield and changes in surface condition as probed by EELS or Auger spectroscopy, since the deexcitation of plasmons or Auger processes may act as a generation channel for the measured secondary electrons. It is worthwhile comparing the sampling depth of the different spectroscopic techniques used in this study in order to correlate the spectral evolution of the argon-sputtered surface with the loss of long-range order (diffraction symmetry), the disruption of short-range order (sp^3-sp^2 bonding) and the suppression of secondary-

electron yield (scattering by surface defects). The sampling depth of EELS using 1000-eV electrons is about 2 nm, while the mean free path for the B (*KVV*) Auger electrons is about 0.6 nm.[33] The mean free path for the low-energy secondary electrons below 20 eV can be higher than 2 nm, but the escape probability is critically dependent on surface defects, long-range order, surface chemical composition, etc. The damage range of 1.5–2-KeV argon ions is in the same order as the sampling depth of 1000-eV EELS based on TRIM88 calculations.[34] Both EELS and *KVV* Auger results have shown that amorphorization of the *c*-BN surface by 0.5–2-KeV argon ions cause an increasing conversion of the surface into sp^2 bonding, while the SEE spectra show that the yield of secondary electrons in the near surface region decreases drastically with argon ion beam energy greater than 1.5 KeV. Since the skin depth of EELS covers the entire thickness of the ion-beam-modified *c*-BN using 0.5–2-KeV argon ions, the evolution of the bulk-plasmon feature E_1 (36.8 eV) reflects the damage range of the argon ions. For example, while low-energy argon-ion beam (>500 eV) can disrupt sp^3 bonding on the surface, its damage range is limited to 1 nm, so the bulk-plasmon peak E_1 remains strong, and is suppressed only by 1.5–2-KeV argon treatment with deeper damage range (> 2.5 nm). The suppression of peak E_1 in Figs. 9(g) and 9(h) following 2-KeV argon treatment is evident of the loss of crystallinity of up to 2.5 nm from the surface, due to the conversion of the near-surface regions into sp^2 amorphous layers. Therefore the regeneration of peak E_1 (bulk plasmon) and suppression of peak P (sp^2 bonding) following hydrogen-plasma treatment in Fig. 9(i) implies that atomic hydrogen is effective in etching away all the amorphorized sp^2 BN layers and to uncover the deeper undamaged crystalline phase. It is interesting to consider that the drastic suppression in secondary yield and the disappearance of peak S_0 (7.5 eV) in the SEE spectra [Figs. 8(g)–8(h)] corresponds to the disappearance of the bulk-plasmon peak E_1 (35 eV) in the EELS spectra [Figs. 9(g)–9(h)]. Whereas higher-energy SEE fine features S_1, S_2, and S_3 are attenuated with short-time and low-energy argon sputtering, suggesting that their disappearance is related to the shorter mean free path of these electrons which cannot escape through the amorphorized surface layers, the SEE peak S_0 parallels the plasmon peak E_1 along the course of the argon sputtering, and both peaks extinguished simultaneously towards the end. We speculate therefore that the secondary-electron peak S_0 has its origins from the plasmon deexcitation processes, which manifest in energy-loss peak E_1. In other words, bulk-plasmon deexcitation process generates secondary electrons that collect at the bottom of conduction band (S_0) prior to their escape into the vacuum.

To test our hypothesis, the EELS spectra of *c*-BN was collected with the primary excitation energy varied between 1000 and 200 eV in order to correlate the plasmon peaks to the total intensity and fine structures of the corresponding SEE spectra. We observed that as the primary excitation energy was decreased from 1000 to 200 eV, the bulk-plasmon peak E_1 became increasingly weaker, along with a parallel suppression in the integral secondary-electron yield and attenuation in the intensity of peak S_0, as shown in Fig 6. We interprete the connection by linking the excitation of the bulk plasmon at 36.8 eV as being the primary true secondary electron production channel. In that context, the near-zero secondary-electron peaks in amorphous carbon thin film[35,36] as well as graphite[37] have also been correlated to plasmon decay.

The short mean free path of the B-*KVV* Auger electrons (0.6 nm) (Ref. 33) means that the line shape is representative of the surface structure up to three atomic layers from the surface. The Auger spectrum of crystalline BN is less well resolved compared to *h*-BN. The main signature for the amorphorization of the surface develops on the right shoulder of the derivative B-*KVV* peaks, in the form of peaks A_5 and A_6 as shown in Fig. 10(b). In the context of *h*-BN, the origin of peaks A_5 and A_6 have been interpreted[2] by the self-convolution of the valence band density of states, or by considering interatomic Auger transitions of the $K_B L^N_{2,3} L^N_{2,3}$ type from electron orbital components. Peak A_4 has been linked to double Auger transition[38] involving a core exciton in the final state while the high-energy peak A_6 may be the direct nonradiative recombination of such an excition. Hydrogen-plasma treatment of the amorphorized surface removes all the fine features A_3–A_8. Therefore, in contrast to the SEE spectra where the fine features become smeared-out following argon sputtering, the Auger B-*KVV* spectrum actually develops sharper features following the amorphorization of the surface. One possible interpretation is that the effect of argon sputtering creates defect as well as π-bonding states, narrows the band gap, and that the richly structured Auger features arise from a self-convolution of these states. An additional observation involves the gradual evolution of the Auger KVV spectra in contrast to the sudden loss of fine structures in the SEE spectra during the earliest stage of sequential argon sputtering. This prompts us to infer that the Auger *KVV* features are sensitive to short-range local order (sp^3–sp^2) which is only gradually disrupted with increasing argon dose while the SEE fine features are sensitive to long-range ordering, which is readily disrupted at the early stage.

D. Possible roles of atomic hydrogen in *c*-BN in growth

Harris *et al.*[39] demonstrated recently that a polycrystalline, mixed sp^2/sp^3 BN film grown heteroepitaxially on Si can be etched by a dilute CH_4H_2 mixture in a hot filament reactor, as is evident from the etching of the film to the bare substrate on some areas. They suggested that the sp^2 phase was preferentially etched. In this study, we observed that by using pure hydrogen plasma, both the sp^2 and sp^3 phases on a single-crystal *c*-BN can be etched. The ability of atomic hydrogen (produced by the dissociation of pure hydrogen in microwave plasma) to etch away sp^2 BN layers on *c*-BN and regenerate crystallinity suggests a possible role of atomic hydrogen as an sp^2 etchant during the vapor phase deposition of *c*-BN. For example, there could be alternative growth and etching cycles for producing a higher purity film. However, we discover in this study that atomic hydrogen is capable of etching the sp^3 layers to restructure the *c*-BN surface as well. This means that the presence of atomic hydrogen during *c*-BN growth will modify the steps distribution and affect the step flow, influencing the morphologies in an unpredictable way. The differing reactivities of

nitrogen- or boron-terminated faces to hydrogen implies that hydrogen etching may selectively promote the appearance of the face that forms the less volatile hydrides. We are currently extending the work to examine the nature of the terminating species on the surface following hydrogen-plasma treatment of *c*-BN. Nevertheless, our results suggest that it may be worthwhile introducing atomic hydrogen and/or hydrogen ions during the vapor phase deposition of *c*-BN.

V. CONCLUSIONS

(1) Atomic hydrogen generated by microwave plasma is capable of structuring the *c*-BN (100) face at temperatures between 700 and 800 °C. The (100) 2×1 face is not stable to hydrogen etching and becomes faceted, finally generating the (111) 1×1 face that is stable to further hydrogen restructuring.

(2) Low-energy (0.5 KeV) argon-ion sputtering destroys the long-range ordering of *c*-BN, which is reflected in the smearing out of the SEE fine structures related to conduction-band states. Higher-energy (1.5–2 KeV) argon sputtering converts the near-surface region into sp^2 bonding. The amorphorized sp^2 BN layers can be effectively removed by hydrogen plasma to regenerate sp^3 crystallinity.

(3) There is a relationship between the integrated secondary-electron yield and the bulk-plasmon peak at 36.8 eV. Our results suggest that the origin of the low-energy secondary electrons in *c*-BN come from the bulk-plasmon deexcitation process.

*Author to whom correspondence should be addressed. Electronic address: ando@nirim.go.jp

[1] R. H. Wentorf, Jr., R. C. Devries, and F. P. Bundy, Science **208**, 873 (1980).
[2] R. Trehan, Y. Lifshitz, and J. W. Rabalais, J. Vac. Sci. Technol. A **8**, 4026 (1990).
[3] J. Costa, E. Bertran, and J. L. Andujar, Diamond Relat. Mater. **5**, 544 (1996).
[4] Z. L. Akkerman, M. L. Kosinova, N. I. Fainer, Yu. M Rumjantse, and N. P. Sysoeva, Thin Solid Films **260**, 156 (1995).
[5] T. Klotzbucher, W. Pfleging, D. A. Wesner, M. Mergens, and E. W. Kreutz, Diamond Relat. Mater. **5**, 525 (1996).
[6] S. Koizumi, T. Murakami, T. Inuzuka, and K. Suzuki, Appl. Phys. Lett. **57**, 563 (1990).
[7] R. C. Mendes, E. J. Corat, V. J. Trava-Airoidi, N. G. Ferreira, N. F. Leite, and K. Iha, Diamond Relat. Mater. **6**, 490 (1997), and references therein.
[8] K. P. Loh, J. S. Foord, R. B. Jackman, and N. K. Singh, Diamond Relat. Mater. **5**, 231 (1996).
[9] T. Sugino, K. Tanioka, S. Kawasaki, and J. Shirafuji, Jpn. J. Appl. Phys. **36**, L463 (1997).
[10] K. P. Loh, J. S. Foord, R. G. Egdell, and R. B. Jackman, Diamond Relat. Mater. **6**, 874 (1997).
[11] K. Osuch and W. S. Verwoerd, Surf. Sci. **285**, 59 (1993).
[12] R. J. Weiss, Philos. Mag. **29**, 1029 (1974).
[13] Y. Mitsuda, T. Yamada, T. J. Chuang, H. Seki, R. P. Chin, J. Y. Huang, and Y. R. Shen, Surf. Sci. Lett. **257**, L633 (1991).
[14] H. Kawarada, H. Sasaki, and A. Sato, Phys. Rev. B **52**, 11 351 (1995).
[15] B. Tuck, J. Mater. Sci. **10**, 321 (1975).
[16] R. J. Nemanich, P. K. Baumann, M. C. Benjamin, S. W. King, J. van der Weide, and R. F. Davies, Diamond Relat. Mater. **5**, 790 (1996).
[17] M. Kagamida, H. Kanda, M. Akaishi, A. Nukui, T. Osawa, and S. Yamaoka, J. Cryst. Growth **94**, 261 (1989).
[18] A. Hoffman, S. Prawer, and R. Kalish, Phys. Rev. B **45**, 12 736 (1992).
[19] H. R. Philipp and E. A. Taft, Phys. Rev. **127**, 159 (1962).
[20] Y. N. Xu and W. Y. Ching, Phys. Rev. B **44**, 7787 (1991).
[21] D. H. Berns and M. A. Capelli, Appl. Phys. Lett. **68**, 2711 (1996).
[22] B. D. Thoms, M. S. Owens, C. Spiro, and J. E. Butler, Appl. Phys. Lett. **65**, 2957 (1994).
[23] O. M. Kuttel, L. Diederich, E. Schaller, O. Carnal, and L. Schlapbach, Surf. Sci. **337**, L812 (1995).
[24] R. E. Rawles, R. Gat, W. G. Morris, and M. P. D'Evelyn, in *Diamond for Electronic Applications*, edited by C. Creifus, A. Collins, C. Beetz, T. Humphreys, K. Das, and P. Pehrsson, MRS Symposium Proceedings No. 416 (Materials Research Society, Pittsburgh, 1996), p. 299.
[25] A. Hoffman, P. Paterson, and S. Prawer, Nucl. Instrum. Methods B **51**, 226 (1990).
[26] A. Hoffman, S. Prawer, and G. Nyberg, J. Phys.: Condens. Matter **2**, 8099 (1990).
[27] A. Hoffman, G. Nyberg, and J. Liesegang, Phys. Rev. B **45**, 5679 (1992).
[28] A. Hoffman, M. Folman, and S. Prawer, Phys. Rev. B **44**, 4640 (1991).
[29] A. Hoffman, S. Prawer, and M. Folman, Appl. Phys. Lett. **58**, 361 (1991).
[30] M. P. Surh, S. G. Louie, and M. L. Cohen, Phys. Rev. B **43**, 9126 (1991).
[31] R. M. Wentzcovitch, K. J. Chang, and M. L. Cohen, Phys. Rev. B **34**, 1071 (1986).
[32] F. J. Himpsel, J. A. Knapp, J. A. van Vechten, and D. E. Eastman, Phys. Rev. B **20**, 624 (1979).
[33] D. R. Penn, J. Electron Spectrosc. Relat. Phenom. **9**, 29 (1976).
[34] A. Hoffman, P. J. K. Paterson, and S. Prawer, Nucl. Instrum. Methods B **52**, 63 (1990).
[35] F. J. Pijper and P. Kruit, Phys. Rev. B **44**, 9192 (1991).
[36] M. R. Scheinfein, J. Drucker, and J. K. Weiss, Phys. Rev. B **47**, 4068 (1993).
[37] A. Hoffman, M. Elbaum, and R. Brener, Phys. Rev. B **48**, 16 078 (1993).
[38] G. Hanke and K. Muller, J. Vac. Sci. Technol. A **2**, 964 (1984).
[39] S. J. Harris, A. M. Weiner, G. L. Doll, and W. J. Meng, J. Mater. Res. **12**, 412 (1997).